WPS1-PR(18) 20425

D Moseev et al.

Collective Thomson Scattering Diagnostic at Wendelstein 7-X

Preprint of Paper to be submitted for publication in
Review of Scientific Instruments

This work has been carried out within the framework of the EUROfusion Consortium and has received funding from the Euratom research and training programme 2014-2018 under grant agreement No 633053. The views and opinions expressed herein do not necessarily reflect those of the European Commission.

Collective Thomson Scattering Diagnostic at Wendelstein 7-X

D Moseev[1], T Stange[1], H P Laqua[1], S Marsen[1], N Schneider[1], I Abramovic[1,2], H Braune[1], W Kasparek[3], S B Korsholm[4], C Lechte[3], F Leipold[4], S K Nielsen[4], M Salewski[4], M Stejner[4], J Rasmussen[4], M Weißgerber[1], R C Wolf[1] and the Wendelstein 7-X team[1]

[1]Max-Planck-Institut für Plasmaphysik, Greifswald and Garching, Germany
[2]Eindhoven University of Technology, Eindhoven, The Netherlands
[3]University of Stuttgart, Stuttgart, Germany
[4]Technical University of Denmark, Kgs. Lyngby, Denmark

E-mail: dmitry.moseev@ipp.mpg.de

Abstract.

A Collective Thomson Scattering (CTS) diagnostic is installed at Wendelstein 7-X for ion temperature measurements in the plasma core. The diagnostic utilizes 140 GHz gyrotrons usually used for electron cyclotron resonance heating as a source of probing radiation. The CTS diagnostic uses a quasi-optical transmission line covering a distance of over 40 m. The same line is used for probe radiation and the radiometer. Here we elaborate on design, installation, and alignment of the diagnostic.

2 May 2018

1. Introduction

The ion temperature T_i is a key parameter to describe plasmas in tokamaks and stellarators. It is important for transport studies, not to mention the fusion yield. Currently the impurity (argon) ion temperature in Wendelstein 7-X (W7-X) is measured by X-ray spectroscopy (XICS) [1–3]. It provides line-integrated measurements which are inverted using a modified Levenberg-Marquardt algorithm into profile measurements. A local ion temperature measurement in the core is important because it provides a constraint for the XICS inversion. Here, the knowledge of the local value of T_i in the center would be of a high value. The collective Thomson scattering (CTS) diagnostic is capable of providing such measurements.

Here we report on the instrumental aspects of the diagnostic. The diagnostic is inspired by the one installed at ASDEX Upgrade [4–9]. The microwave-based CTS diagnostic has proven its capability for ion temperature measurements on several tokamaks [10, 11] and stellarators [12, 13]. CTS measures directly the bulk plasma (i.e. usually deuterium,

helium, or hydrogen) temperature rather than the temperature of an impurity. These two temperatures can sometimes be quite different [14]. Recently the feasibility of T_i measurements by CTS, having the second harmonic electron-cyclotron resonance in direct view of the receiver, was demonstrated on ASDEX Upgrade [15, 16].

CTS is scattering of electromagnetic waves off the collective fluctuations in the plasma. The measurements are done using a probing beam with the wave vector $\vec{k}^i$, which is scattered on fluctuations in the plasma, and a receiver beam with the wave vector $\vec{k}^s$ that detects scattered waves. Salpeter [17] found that if $k^\delta \lambda_D \ll 1$, where k^δ is the magnitude of $\vec{k}^\delta = \vec{k}^s - \vec{k}^i$, and λ_D is the Debye length, the spectrum of the scattering radiation bears signatures of collective effects in the plasma. The CTS diagnostic measures a spectrum of scattered microwaves. Generally, the spectral shape and magnitude depends on the scattering geometry and many plasma parameters: the ion temperature T_i, the electron temperature T_e, the electron density n_e and the effective charge Z_{eff} etc. Comprehensive models [18] exist which allow inference of the plasma parameters by solving an inverse problem. Bayesian inference using the Minerva framework [19] is employed for T_i measurements in W7-X [20]. Neural network analysis will also be used for the fast evaluation of the ion temperature in W7-X [21]. The sensitivity of the diagnostic to the ion temperature is illustrated by the scattering functions in Fig. 1 which describe the spectrum formation in CTS measurements. We use O-O mode scattering of the probing radiation of 140 GHz. The electron temperature is 8 keV, and the ion temperatures are 4 keV and 8 keV. One can clearly see the influence of ion temperature on the shape of the spectrum.

The design aspects of the CTS diagnostic for W7-X are discussed in Section 2. Section 3 addresses the alignment of the transmission line. Section 4 concludes this publication.

2. Design of the CTS diagnostic

The W7-X electron cyclotron resonance heating (ECRH) system consists of ten gyrotrons working at 140 GHz, a quasi-optical transmission line, and several launchers located in modules 1 and 5 of the stellarator, as schematically shown in Fig. 2. A more detailed description of the ECRH setup is given in reference [22]. The CTS diagnostic extensively uses the ECRH infrastructure of W7-X. The two gyrotrons A1 and B1 from the ECRH installation are used as sources of the probing radiation for CTS. The preinstalled ECRH launcher mirror F1 is used as front-end receiver mirror. The number of installed ECRH launchers per module is one more than the number of gyrotrons in the corresponding module. The extra launchers are reserved for future updates of the ECRH installation. The main part of the transmission line from the matching optics unit (MOU) at the end of the transmission line to the ECRH tower in module 1 is also shared.

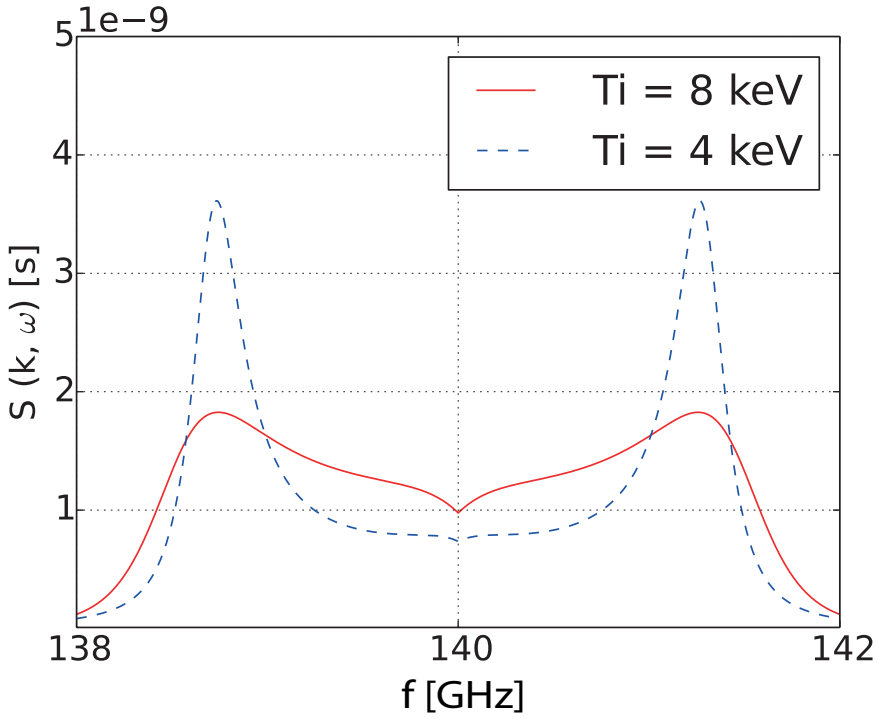

Figure 1. Two example spectra where the ion temperature is varied (4 and 8 keV), having the other parameters fixed: $T_e = 8$ keV, $B = 2.4$ T, $n_e = 10^{20}$ m^{-3}, $f_{probe} = 140$ GHz.

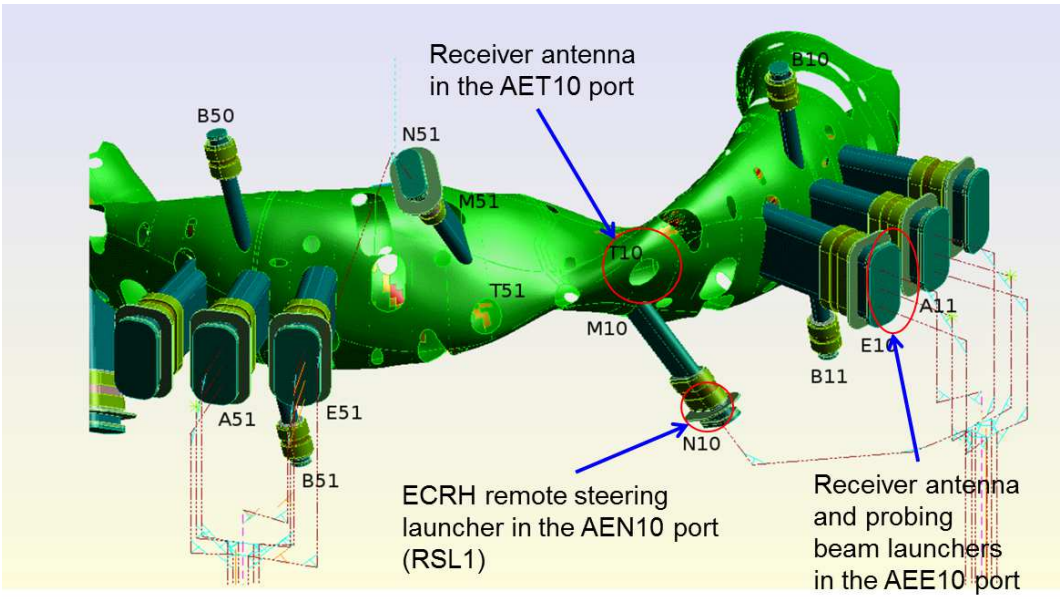

Figure 2. A CAD overview of a part of the W7-X vessel with the ECRH launchers and CTS receiver antennas.

The diagnostic is able to collect scattered microwaves from two different locations in the plasma, namely from the port AEE10 in the bean-shaped cross-section and from the port AET10 in the triangular cross-section. Both ports are located in Module 1. These cross-sections are illustrated in Fig. 3. The ECRH launchers in the AEE10 port (bean-shaped cross-section) are equipped with the mirrors that have 2D steering capabilities, which allows the exploration of scattering geometries with different angle of $\vec{k^{\delta}}$ to the external magnetic field. In the triangular cross-section both probing and receiver beams can be steered in one dimension only.
Due to the topology of the magnetic field, better resolution of T_i measurements in the magnetic flux co-ordinates can be achieved in the triangular cross-section. The exact values of achievable resolution depend on the exact scattering geometry and the chosen cross-section and varies in the range $\Delta\rho_t \approx 0.1 - 0.5$.
The diagnostic utilizes the remote steering launcher (RSL) [22, 23] in the AEN10 port (Module 1) in order to transmit the probing radiation into the triangular cross-section. The B1 gyrotron has a possibility to be switched to the remote steering antenna in the triangular cross-section in module 1.

In the bean-shaped cross-section the second harmonic 140 GHz electron cyclotron (EC) resonant surface crosses the plasma center from top to bottom. This implies that the scattering volume cannot be placed in the very core. The electron cyclotron emission (ECE) background which is received by the diagnostic is also very high and corresponds to the electron temperature near plasma center, which is in the range of several keV. In the triangular cross-section the receiver beam at its first pass does not cross the resonance surface and one might expect lower levels of the received ECE background radiation. However, reflected ECE enters the receiver in the triangular cross-section as well the background is only reduced by a few percent. Nonetheless, a clear advantage of the triangular cross-section is the accessibility of the plasma center for the T_i measurements.

2.1. Transmission line

The CTS diagnostic at Wendelstein 7-X uses the standard ECRH system to provide the probe radiation. Here we focus on the transmission of the received radiation from the plasma to the radiometer. The receiver is connected via a matching optics unit and a quasi-optical transmission line to the receiver mirrors in module 1 in the triangular and bean-shaped cross-sections. An overview of the transmission line is shown in Fig. 4. Switching between the two cross-sections is done by the removable mirror in the vicinity of the launcher in the bean-shaped cross-section, in the ECRH Tower 1. Switching can be performed whenever there is an access to the torus hall. A detailed view of the front-end part of the diagnostic is shown in Fig. 5. A general overview is shown in Fig. 5(a). On the left one can see the ECRH tower where the last stage of

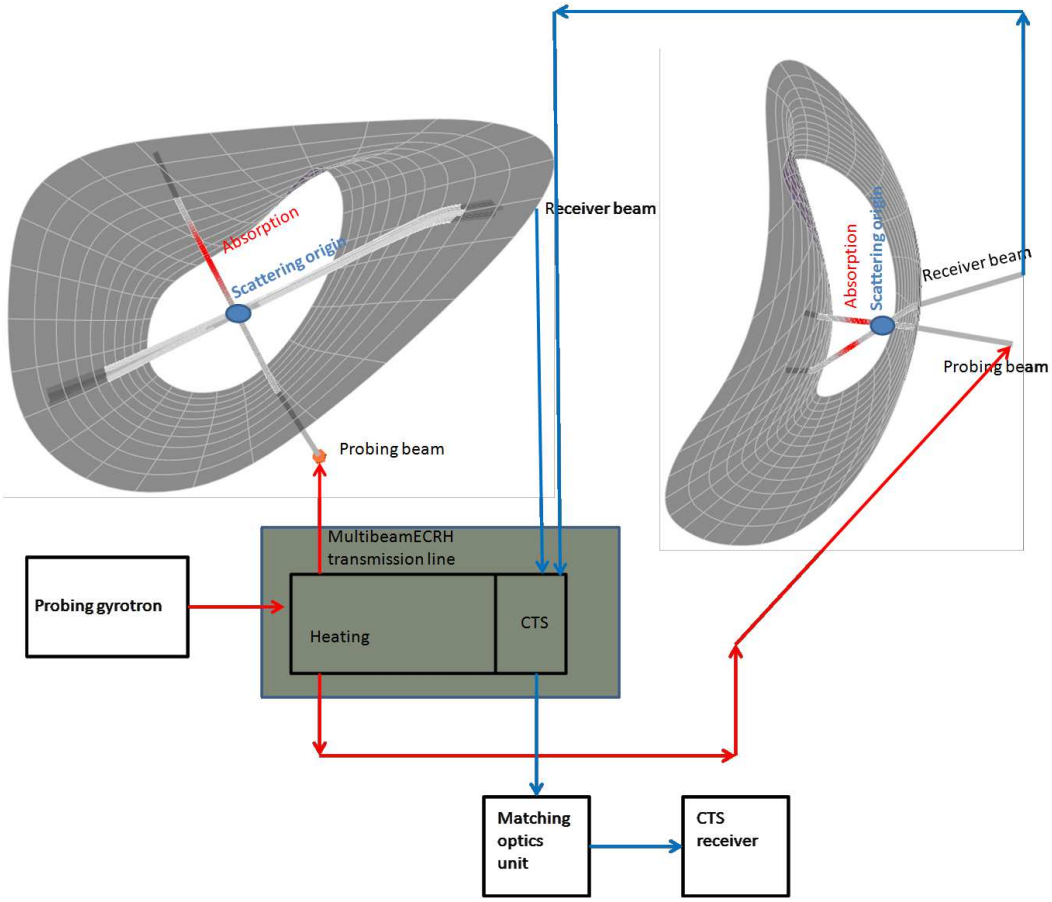

Figure 3. Diagram of the CTS diagnostic. Two stellarator cross-sections are shown where the CTS measurements are performed. On each of the cross-sections, a last closed flux surface is indicated (gray meshed surface). Two beams are assigned as a probing beam and as a receiving beam in each cross-section. Red coloring along the beam lines in the plasma shows the position of electron cyclotron absorption and emission for 140 GHz probing and receiver beams, respectively. The location where two beams intersect in the plasma is denoted as the origin of the measured scattering radiation. Red arrows indicate a direction of the power flow from the gyrotron to the plasma via the multi-beam quasi-optical ECRH transmission line. The blue arrows show the power flow of the scattering radiation towards the CTS receiver (heterodyne radiometer) via the multi-beam quasi-optical ECRH transmission line and the matching optics unit.

the quasi-optical transmission line, launching optics for ECRH, and receiving optics for CTS (bean-shaped cross-section) are located. In Fig. 5(b) a removable mirror is shown which serves as a switch between two CTS views. On the same figure one can see a port plug-in for the CTS diagnostic in the triangular cross-section. Fig. 5(c) shows the antenna in more detail. The confocal mirror system images the pivot point of the receiver beam near to the plasma onto the only steerable mirror, which is situated in the air outside the vacuum window. Therefore, no movable parts are needed in vacuum. The steerable mirror allows beam steering in one plane only, the extreme positions of the beam and the mirror are shown in the figure. The front-end part of the CTS system in

the bean-shaped cross-section is shown in Fig. 5(d). The mirrors for CTS and ECRH are identical and have large steering flexibility.

The overview of the modified transmission line is shown in Fig. 4. There the locations of the receiving optics is schematically depicted on the left side of the picture and denoted by the name of the ports where the launching and receiving optics is located: AEE10 (see Fig. 5(d)) for the bean-shaped cross-section and AEN10 - AET10 for the launcher and the receiver, respectively) for the triangular cross-section, see Fig. 5(c). When scattered radiation is collected from the bean-shaped cross-section, microwaves are transmitted from the receiving mirror to mirror M14. In this configuration, the removable mirror M15 is removed from the transmission line. When scattered microwaves are collected from the triangular cross-section, the radiation comes from the port plug-in shown in Fig. 5(b) and the received beam is selected by the steerable mirror M17 located outside of the vacuum vessel. The scattering signal is guided to the M14 mirror via mirrors M16 and M15. From this mirror onward there is no difference for the beam paths originating from the bean-shaped and triangular cross-sections. The mirror M12 belongs to the beam-dividing optics - a set of mirrors where the multi-beam is divided into individual ECRH beams or receiving beams and transmitted to launchers. Optically it is identical to the beam-combining optics, where individual microwave beams are collected for transmission in the multi-beam part of the transmission line, see Fig. 6(a). The terms "combining" and "dividing" were introduced with respect to the ECRH beams which travel from gyrotrons to the plasma. We will stick to these names even for the received CTS radiation propagating in the opposite direction. After passing M12 the received CTS radiation shares the same multi-beam mirrors M5-M11 with the gyrotrons in module 1, including the probing beam. In no other CTS diagnostic do the receiver and the probing beams share the same mirrors simultaneously. Although the intensity of the beams differs by 120-140 dB it imposes no practical difficulties. The multi-beam mirror and its dimensions are shown on Fig. 6(b). Mirror M4 is a part of the beam combining optics, where the ECRH and CTS beams are again split into the individual transmission lines, see Fig. 6(a). The radiation from mirror M4 travels through mirrors M3Z1-4 (Z stands for zig-zag) to mirror M3. The set of mirrors termed M3Z is necessary to bypass obstacles on the beam propagation path, see Fig. 6(c). Mirror M3 guides the radiation to polarizer plates P2 and P1 which emulate a quarter-wave plate and a half-wave plate, respectively [24]. The polarized radiation is guided through mirrors M2 and M1 into the CTS receiver, which is located in the Faraday cage built for the foreseen F1 gyrotron and is separated by a 40 cm thick concrete wall from the quasi-optical transmission line.

2.2. CTS Receiver

The CTS receiver at W7-X is a heterodyne radiometer and is installed in a gyrotron cage outside of the torus hall and the ECRH transmission lines. The design is similar to the

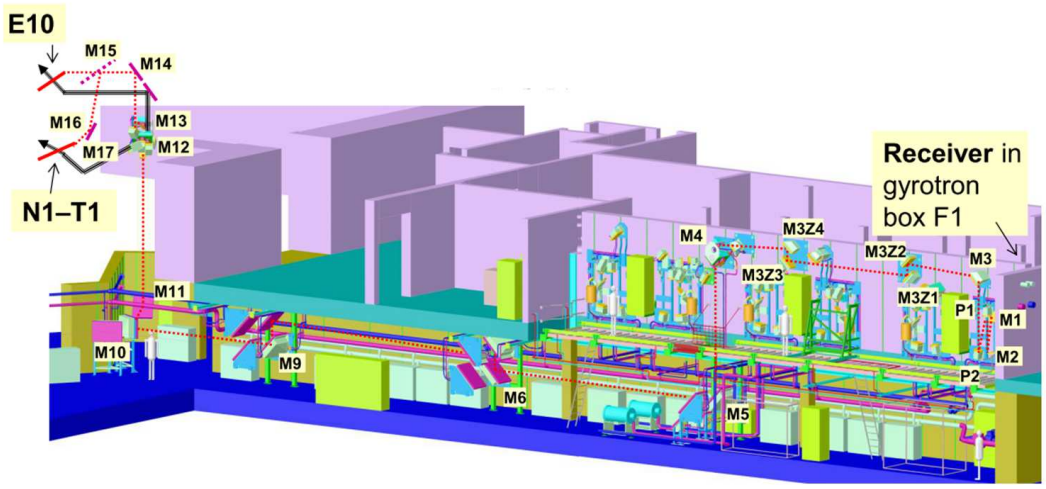

Figure 4. A detailed representation of the receiving part of the CTS transmission line.

one installed on ASDEX Upgrade and previously on TEXTOR [6,25,26]. The receiver is equipped with a 16 channel filter bank for commissioning covering the frequency range 135-145 GHz, and a fast analog-to-digital converter National Instruments model PXIe-5186 with a sampling rate of 6.25 (max. 12.5) Gsamples per second and a bandwidth of 5 GHz.

2.3. Remote steering antenna

A remote steering quasi-optical antenna is designed and manufactured for the CTS diagnostic in port AET10 (triangular cross-section). It is shown in Fig. 5(c). The antenna provides optical imaging from a location near the pivot point at the end of the antenna (marked as a red dot on the left side of the figure) to the center of the vacuum window of the port (red dot on the right side of the figure). The antenna has four focusing mirrors, five plane reflectors, and a steerable mirror. Such a long construction is needed to close the gap between the cryostat and the plasma vessel.
The steerable mirror located outside of the plasma vacuum moves in the slotted link by a linear driver. It allows steering the received beam $\pm 15^\circ$ in one dimension. The amount of the mode loss of the Gaussian beam depends on the steering angle. However, in the entire range of steering angles the mode loss does not exceed 0.4%.
Prior to its installation into W7-X, the remote steering antenna was tested in the laboratory using a low-power microwave source and the transmitted beam quality, as well as the steering capabilities were found in agreement with the design.

2.4. Distribution of stray radiation in the port plug-in

The CTS diagnostic is designed to run in steady-state plasmas of W7-X which last for 30 minutes. This implies that the CTS antenna plug-in in the AET10 port needs active

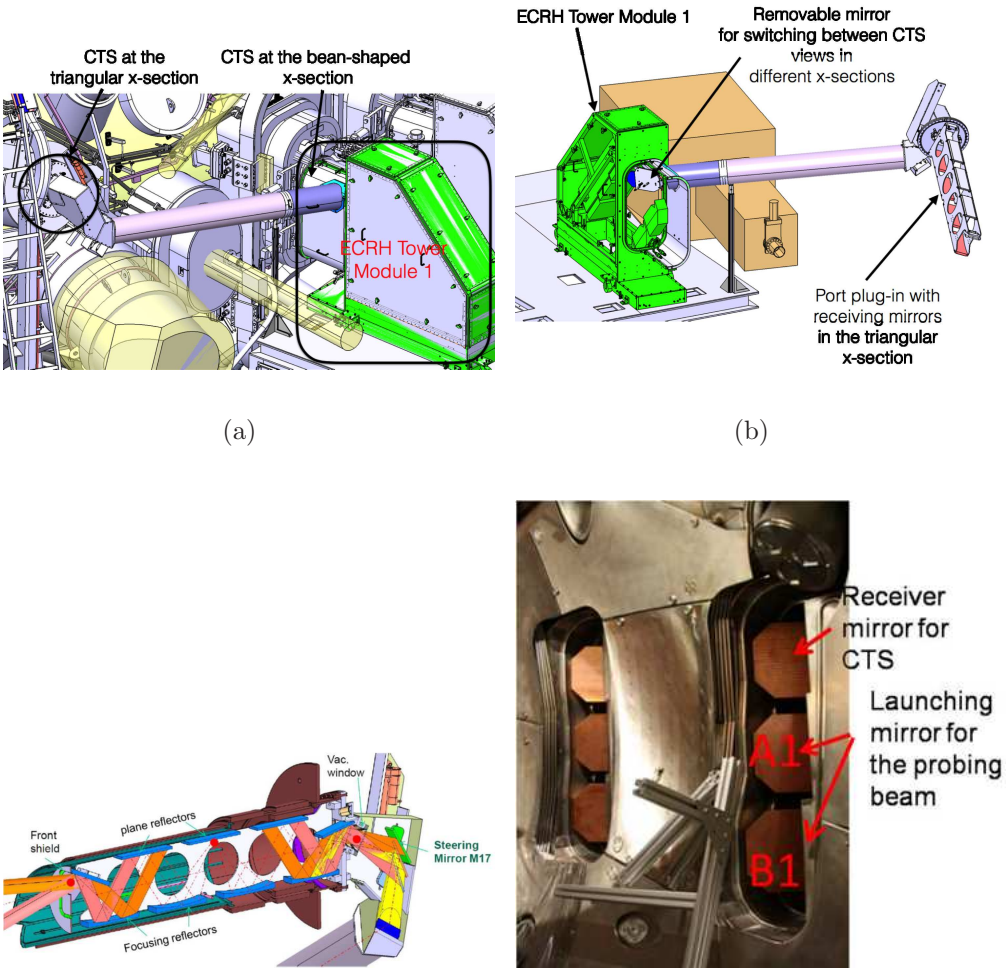

Figure 5. CTS infrastructure in the W7-X torus hall. (a) Overview of the CTS installation in the torus hall. The CTS receiver mirrors are located in the ECRH tower in the bean-shaped cross-section, port AEE10, and in the port in the triangular cross-section AET10. The cryostat of W7-X is on the background of the image. (b) Another view of the CTS installation taken from the location of the W7-X vessel (not shown). A removable mirror (M15) in the ECRH tower which enables switching between two different CTS views is shown, as well as a port plug-in for the CTS view in the triangular cross-section. (c) A closer look at the port plug-in for the CTS view in triangular cross-section. A remote steering concept is implemented: the only movable mirror is located in ambient air and couples microwaves from the plug-in further into the transmission line. The steerable mirror is shown at its extreme steering positions, and the corresponding received microwave beams are schematically depicted. (d) A photograph of the in-vessel launching and receiving mirrors for the CTS view in the bean-shaped cross-section.

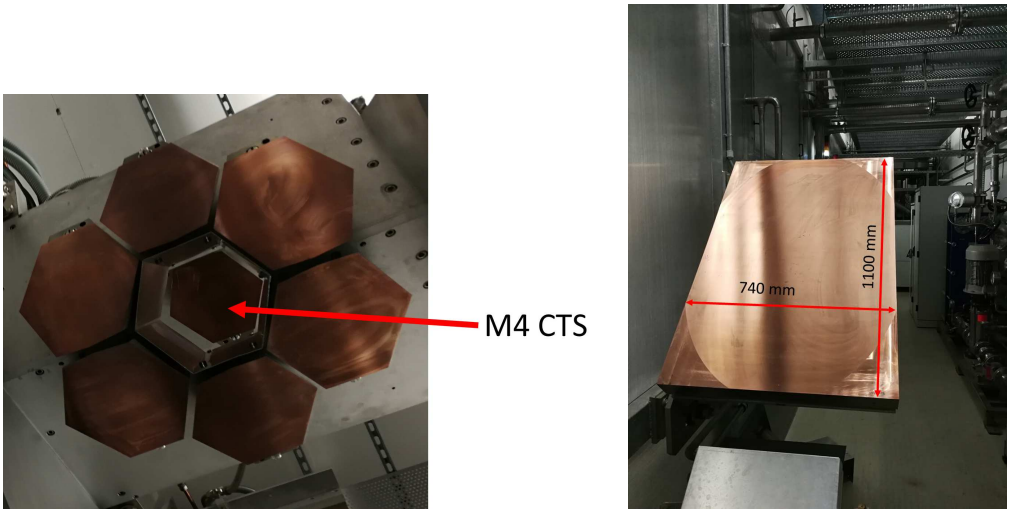

(a) (b)

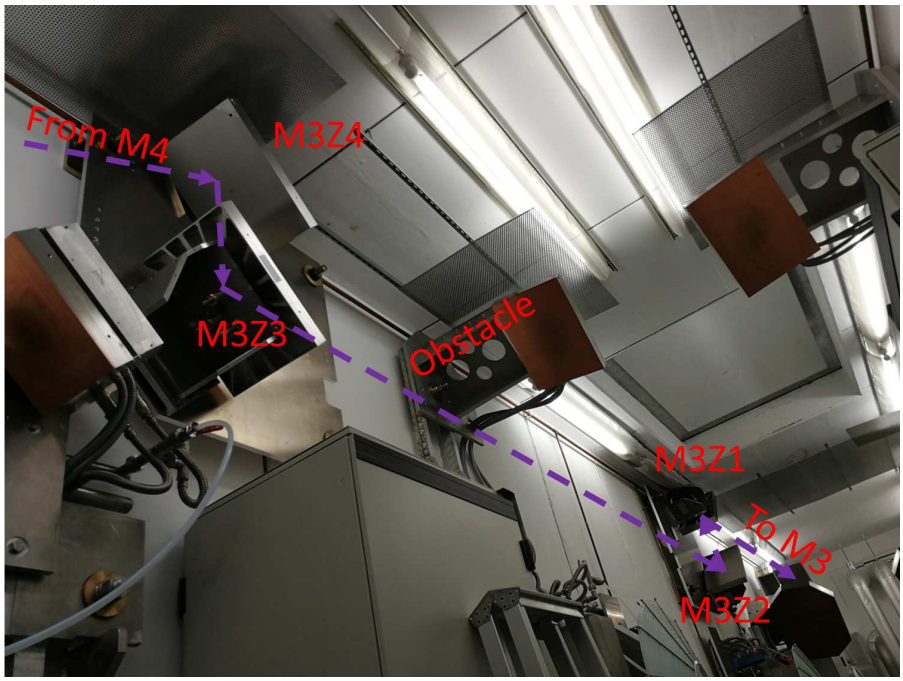

(c)

Figure 6. Some mirrors in the quasi-optical transmission line. (a) Beam-combining optics (M4) collects radiation from all the sources in module 1 and directs it to the multi-beam part of the transmission line. The received CTS beam (travelling in the opposite direction) is selected from the multi-beam part of the transmission line and directed to the receiver. Mirror M4 for the CTS transmission line is in the center. (b) M5, the first mirror of the multi-beam part of the quasi-optical transmission line for module 1. It can transmit up to seven beams simultaneously. (c) Set of zig-zag mirrors termed M3Z, which allow the received beam to bypass an obstacle on its way to M2.

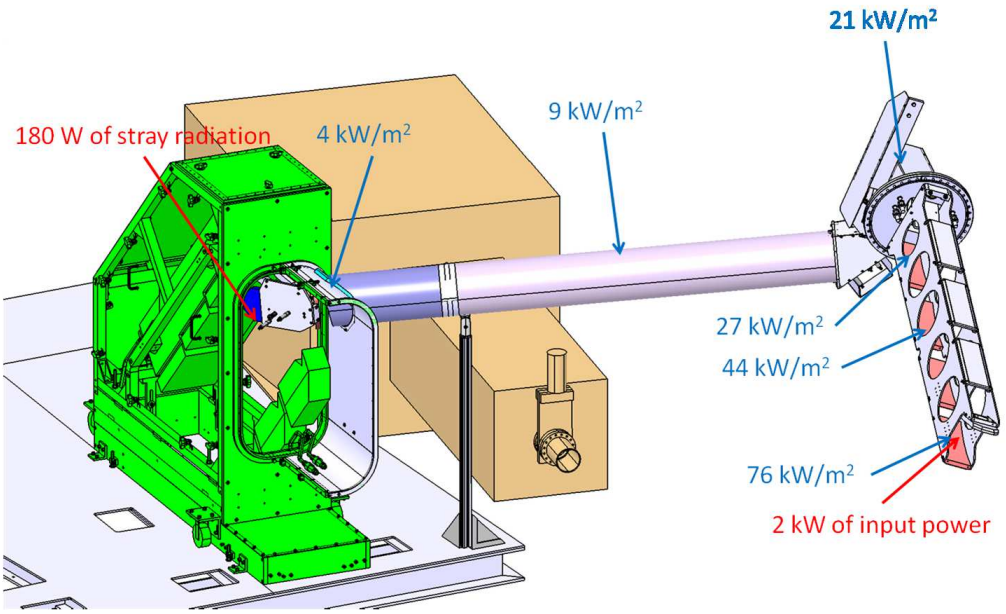

Figure 7. The distribution of stray radiation in the transmission line from the port plug-in in the triangular cross-section to the ECRH tower.

cooling. The other receiver mirror location was already designed to have active cooling as it is part of the ECRH launcher. In the case of a receiver mirror in the triangular cross-section, the main heating source is stray radiation. In order to investigate where most of the stray radiation is absorbed, a dedicated analysis is conducted. In the worst case scenario, when 10% of the entire gyrotron power is not absorbed and bounces in the vessel, referred to a stray radiation, the antenna plug-in receives around 2 kW of microwave stray radiation. Stray radiation from ECE is not taken into account because of its insignificance in the W7-X plasmas [27]. The distribution of stray radiation in the port plug-in and in the transmission line from the port in the triangular cross-section to the ECRH tower in module 1 is calculated using a multicavity model [28]. The model has proven its validity in the OP1.1 campaign [29] and is used to simulate the stray radiation loads in ITER. The distribution is shown in Fig. 7. The modeling shows that less than 10% of the input power, 180 W out of 2 kW, will be transmitted into the ECRH tower which has an absorbing wall capable of dissipating orders of magnitude more. Most of the power, approximately 75%, is expected to be absorbed in the plug-in. The analysis shows that for steady-state operation the plug-in has to be actively cooled, which unfortunately made the design of the plug-in more complicated. In the experimental campaign OP1.2 no steady-state operation is planned and active cooling is not necessary: the total injected energy into the plasma in OP1.2 is not allowed to exceed 80 MJ per discharge, which corresponds to about 10 s of operation at full ECRH power. In this case, the total energy that might enter the port plug-in in terms of stray radiation is not more than 20 kJ which is not enough to overheat the components.

3. Alignment of the transmission line

The alignment of the transmission line is crucial for the successful operation of the diagnostic, since the measured signal originates from the overlap region between the probing and the receiver beams. Moreover, in the quasi-optical transmission line a misalignment between the mirrors may lead to a total loss of the beam in severe cases, i.e. the received signal would not originate from the plasma at all.
The alignment procedure consists of two methodologically different tasks: aligning the mirrors of the transmission line, so that the microwave (Gaussian) beam may travel from the receiver to the last mirror of the transmission line and, secondly, mapping the motor position of the steerable mirror onto the receiver beam trajectory in the vacuum vessel.
The microwave alignment of the transmission line is done by means of thermography. A 10 W microwave source is connected to the horn of the receiver, so that the receiver becomes a transmitter. A microwave target, made of wet laminated paper with glued reflective aluminum foil markers, is fixed at the center of the first mirror. The beam pattern on the target is measured by an infrared camera monitoring the thermal footprint of the beam. The mirror is shifted in such a way that the beam is centered. When done, the microwave target is fixed on the next mirror and the previous mirror is tilted around the normal to its surface, originating in the center of the beam, so that the beam is centered on the next mirror. This procedure continues step by step from mirror M1 to M5 and then from M12 to the end of the transmission line, see Fig. 4. The multi-beam transmission line did not need to be aligned specifically for CTS since it has already been aligned for the ECRH system. Generally, the multi-beam part of the transmission line needs to be aligned for two beams only and it becomes automatically aligned for all other beams transmitted through it (in total up to seven beams). An example of an alignment setup is shown in Fig. 8(a). An example of a thermographic measurement of the microwave beam on a wet-paper target is shown in Fig. 8(b).

The in-vessel alignment is done by means of a double-sided laser beam. Small optical reflectors are installed in the centers of the last two microwave mirrors and a semi-transparent target is mounted on the vacuum window. The laser is installed inside the vacuum vessel in such a way, that its beam, after being reflected from the reflectors on the microwave mirrors, meets the center of the vacuum window. Since the laser is double-sided, the interception point of the second beam on the high-field-side wall is recorded. Therefore, the motor positions of the mirror drive are mapped to the launching (or receiving) directions of the microwave beam. These mappings are done for all ten launchers in the bean-shaped cross-sections. The laser mapping is checked by the in-vessel microwave alignment at eleven different locations, when the microwave target is placed on the high-field-side wall. It shows that the laser mapping technique is adequately suited for the aiming of the microwave beam, see Fig. 9 as an example.

Fig. 10 shows the obtained mapping between the motor drive positions of the last steerable mirror in the CTS transmission line in the AEE10 port (bean-shaped

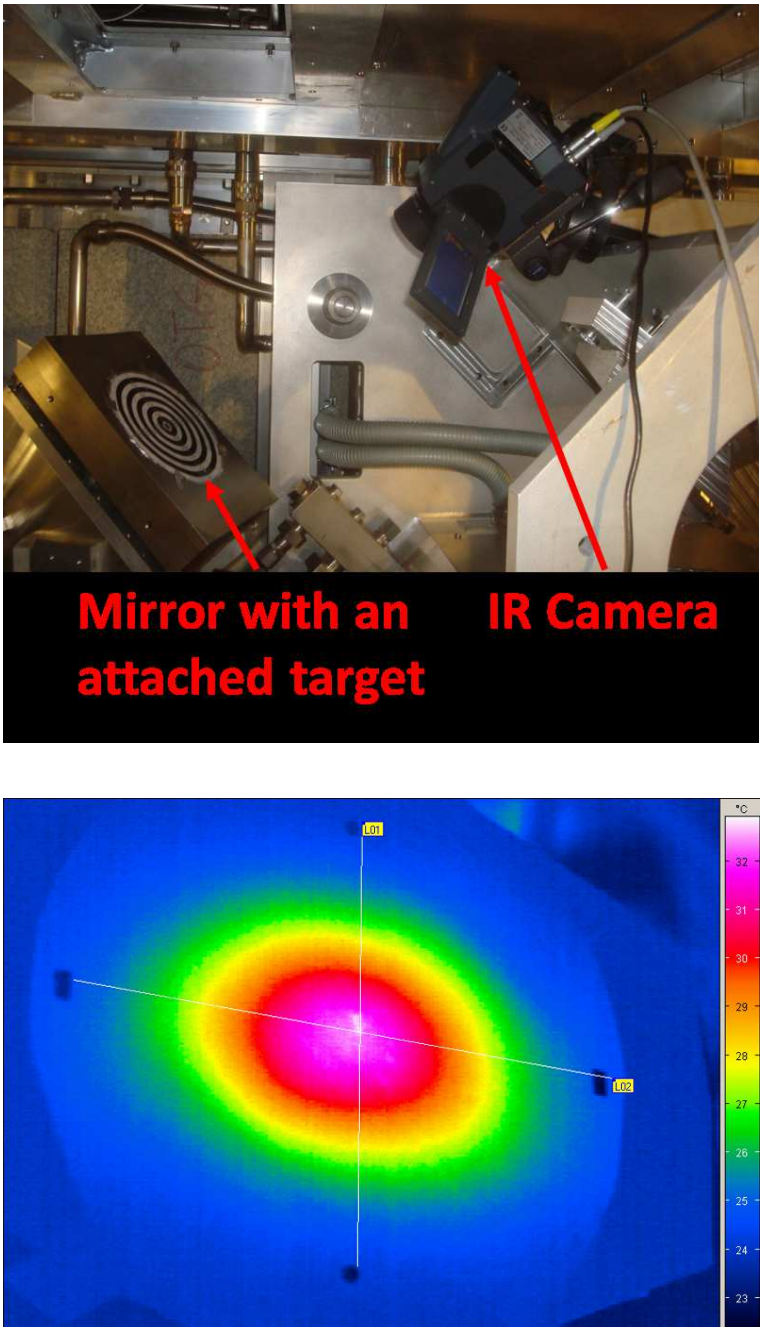

Figure 8. (a) An example of the microwave alignment setup at mirror M13 of the CTS receiver transmission line; (b) an infrared image of the microwave beam on mirror M4 after adjustment of the previous mirror M3Z4.

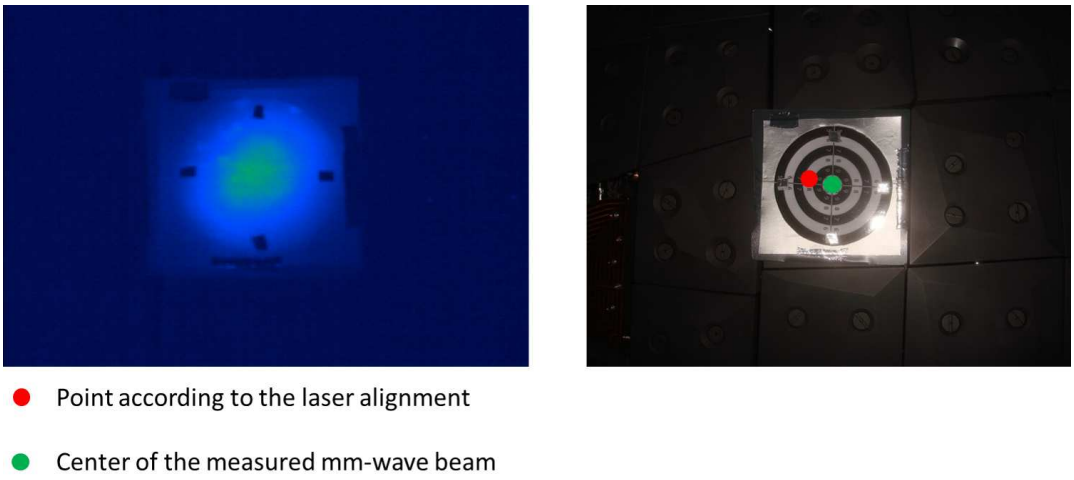

Figure 9. Comparison of the laser alignment with the microwave alignment. (left) An infrared image of the microwave beam on the target on a high-field-side wall. (right) A center of the microwave beam obtained from the measurements (green dot) and the expected position of the beam center, calculated from the laser alignment (red dot) over-plotted on the wet-paper target on the high-field-side wall, the same as on the left panel. The reflective markers on the target are located 50 mm from the center of the target.

cross-section) to the beam-aiming parameters: the projection angle of the beam onto the equatorial plane to the normal to the magnetic axis (ϕ_{tor}, °) and the vertical displacement of the microwave beam with respect to the magnetic axis (Z_{off}, mm).

The CTS receiver mirror in the triangular cross-section (AET10 port) is capable of 1D motion only, therefore the laser alignment is omitted.

4. Conclusions

A CTS diagnostic for ion temperature measurements on Wendelstein 7-X has been designed and installed on Wendelstein 7-X. The diagnostic features a highly sensitive, high-resolution heterodyne receiver. A heating gyrotron at 140 GHz is a source of the probing radiation. The CTS receiver beam is transmitted to the receiver using shared quasi-optical transmission line with the ECRH gyrotrons from module 1, including its own probing beam.

The diagnostic has two viewing locations in the cross-sections with different magnetic topologies. In the triangular cross-section, the plasma center is available for measurements. In the bean-shaped cross-section at the standard magnetic field, the plasma center is unavailable due to the presence of the cold 140 GHz ECE resonance. The resolution in the flux-surface co-ordinates in the triangular cross-section is generally better in comparison to the bean-shaped cross-section due to the different magnetic field topology. The exact values of achievable spatial resolution depend on the exact geometry settings and chosen cross-section and range $\Delta\rho_t \approx 0.1 - 0.5$.

The receiver beam in the triangular-shaped cross-section does not cross the ECE

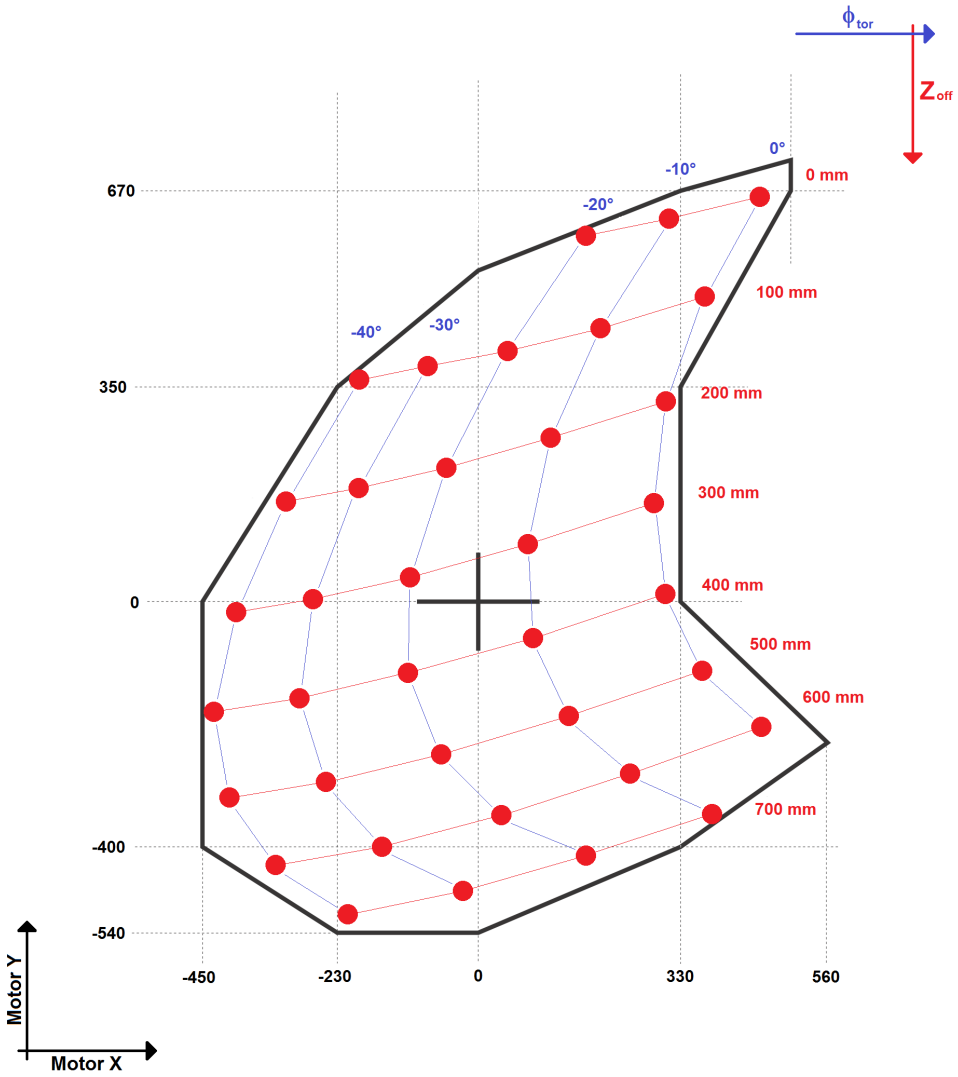

Figure 10. A mapping between the motor drive positions X and Y of the steerable mirror of the CTS receiver in the bean-shaped cross-section to the beam-aiming parameters ϕ_{tor} and Z_{off}. Black solid line shows the operational limits of the steerable mirror.

resonance layer on the first pass one might expect low level of the received ECE background. However, due to the highly reflecting walls of the vacuum vessel, the ECE background is received after reflections off the wall. It was also noted during the experimental campaign OP1.2a, that there is no notable difference in the strength of the received background radiation in the X- or O-mode, also due to the reflections. The situation will be different as soon as W7-X operates at densities above $1.2{\cdot}10^{20}$ m^{-3}, which is a cut-off frequency for the X-mode radiation.

Acknowledgments

This work has been carried out within the framework of the EUROfusion Consortium and has received funding from the Euratom research and training programme 20142018 under grant agreement No. 633053. The views and opinions expressed herein do not necessarily reflect those of the European Commission.

References

[1] N A Pablant, M Bitter, R Burhenn, L Delgado-Aparicio, R Ellis, D Gates, M Goto, K W Hill, A Langenberg, S Lazerson, M Mardenfeld, S Morita, G H Neilson, T Oishi, and T S Pedersen. Measurement of core plasma temperature and rotation on W7-X made available by the x-ray imaging crystal spectrometer (XICS). In *41st EPS Conference on Plasma Physics*, page P1.076, Berlin, Germany, 2014.

[2] N. A. Pablant, R. E. Bell, M. Bitter, L. Delgado-Aparicio, K. W. Hill, S. Lazerson, and S. Morita. Tomographic inversion techniques incorporating physical constraints for line integrated spectroscopy in stellarators and tokamaks. *Review of Scientific Instruments*, 85(11):11E424, nov 2014.

[3] N. A. Pablant, M. Bitter, L. Delgado-Aparicio, M. Goto, K. W. Hill, S. Lazerson, S. Morita, A. L. Roquemore, D. Gates, D. Monticello, H. Nielson, A. Reiman, M. Reinke, J. E. Rice, and H. Yamada. Layout and results from the initial operation of the high-resolution x-ray imaging crystal spectrometer on the Large Helical Device. *Review of Scientific Instruments*, 83(8):083506, aug 2012.

[4] F Meo, H Bindslev, S B Korsholm, V Furtula, F Leuterer, F Leipold, P K Michelsen, S K Nielsen, M Salewski, J Stober, D Wagner, and P Woskov. Commissioning activities and first results from the collective Thomson scattering diagnostic on ASDEX Upgrade (invited). *The Review of scientific instruments*, 79(10):10E501, oct 2008.

[5] M Salewski, F Meo, M Stejner, O Asunta, H Bindslev, V Furtula, S B Korsholm, T Kurki-Suonio, F Leipold, F Leuterer, P K Michelsen, D Moseev, S K Nielsen, J Stober, G Tardini, D Wagner, and P Woskov. Comparison of fast ion collective Thomson scattering measurements at ASDEX Upgrade with numerical simulations. *Nuclear Fusion*, 50(3):035012, mar 2010.

[6] V Furtula, M Salewski, F Leipold, P K Michelsen, S B Korsholm, F Meo, D Moseev, S K Nielsen, M Stejner, and T Johansen. Design and performance of the collective Thomson scattering receiver at ASDEX Upgrade. *Review of Scientific Instruments*, 83(1):013507, 2012.

[7] J Rasmussen, S K Nielsen, M Stejner, B Geiger, M Salewski, A S Jacobsen, S B Korsholm, F Leipold, P K Michelsen, D Moseev, M Schubert, J Stober, G Tardini, and D Wagner. Consistency between real and synthetic fast-ion measurements at ASDEX Upgrade. *Plasma Physics and Controlled Fusion*, 57(7):075014, jul 2015.

[8] S K Nielsen, M Stejner, J Rasmussen, A S Jacobsen, S B Korsholm, F Leipold, M Maraschek, F Meo, P K Michelsen, D Moseev, M Salewski, M Schubert, J Stober, W Suttrop, G Tardini, and D Wagner. Measurements of the fast-ion distribution function at ASDEX upgrade by collective Thomson scattering (CTS) using active and passive views. *Plasma Physics and Controlled Fusion*, 57(3):035009, mar 2015.

[9] M Stejner, S K Nielsen, A S Jacobsen, S B Korsholm, F Leipold, R M McDermott, P K Michelsen, J Rasmussen, M Salewski, M Schubert, J Stober, and D H Wagner. Plasma rotation and ion temperature measurements by collective Thomson scattering at ASDEX Upgrade. *Plasma Physics and Controlled Fusion*, 57(6):062001, jun 2015.

[10] M Stejner, M Salewski, S B Korsholm, H Bindslev, E Delabie, F Leipold, F Meo, P K Michelsen, D Moseev, S K Nielsen, A Bürger, and M de Baar. Measurements of ion temperature and plasma

hydrogenic composition by collective Thomson scattering in neutral beam heated discharges at TEXTOR. *Plasma Physics and Controlled Fusion*, 55(8):085002, aug 2013.

[11] M Stejner, S Nielsen, A S Jacobsen, S B Korsholm, F Leipold, F Meo, P K Michelsen, D Moseev, J Rasmussen, M Salewski, M Schubert, J Stober, and D H Wagner. Resolving the bulk ion region of millimeter-wave collective Thomson scattering spectra at ASDEX Upgrade. *The Review of scientific instruments*, 85(9):093504, sep 2014.

[12] M. Nishiura, S. Kubo, K. Tanaka, R. Seki, S. Ogasawara, T. Shimozuma, K. Okada, S. Kobayashi, T. Mutoh, K. Kawahata, T. Watari, T. Saito, Y. Tatematsu, S.B. Korsholm, and M. Salewski. Spectrum response and analysis of 77 GHz band collective Thomson scattering diagnostic for bulk and fast ions in LHD plasmas. *Nuclear Fusion*, 54(2):023006, feb 2014.

[13] E V Suvorov, V Erckmann, E Holzhauer, W Kasparek, Y A Dryagin, S E Fil'chenkov, A A Fraiman, T Geist, M Kick, L M Kukin, A V Kostrov, L V Lubyako, A M Shtanyuk, N K Skalyga, and O B Smolyakova. Ion temperature and beam-driven plasma waves from collective scattering of gyrotron radiation in W7-AS. *Plasma Physics and Controlled Fusion*, 37(11):1207–1213, 1995.

[14] M. Salewski, B. Geiger, A.S. Jacobsen, I. Abramovic, S.B. Korsholm, F. Leipold, B. Madsen, J. Madsen, R.M. McDermott, D. Moseev, S.K. Nielsen, M. Nocente, J. Rasmussen, M. Stejner, M. Weiland, The EUROfusion MST1 Team, and The ASDEX Upgrade Team. Deuterium temperature, drift velocity, and density measurements in non-Maxwellian plasmas at ASDEX Upgrade. *Nuclear Fusion*, 58(3):036017, mar 2018.

[15] M Stejner, J. Rasmussen, S. Nielsen, A. Jacobsen, S. B. Korsholm, F. Leipold, R. M. McDermott, M. Salewski, M. Schubert, J. Stober, and D.H. Wagner. Determining main-ion temperatures and rotation rates from scattering of electron cyclotron heating waves in ASDEX Upgrade. *submitted to Plasma Physics and Controlled Fusion*, 2016.

[16] M. Stejner, S.K. Nielsen, A.S. Jacobsen, S.B. Korsholm, and F. Leipold. 41st International Conference on Infrared, Millimeter and Terahertz Waves. In *Measuring main-ion temperatures in ASDEX Upgrade using scattering of ECRH radiation*, Copenhagen, Denmark, 2016.

[17] E E Salpeter. Electron Density Fluctuations in a Plasma. *Physical Review*, 120(3):1528, 1960.

[18] H Bindslev. A quantitative study of scattering from electromagnetic fluctuations in plasmas. *Journal of Atmospheric and Terrestrial Physics*, 58(8):983–989, jul 1996.

[19] J. Svensson, O. Ford, D.C. McDonald, A. Meakins, A. Werner, M. Brix, A. Boboc, M. Beurskens, and JET EFDA Contributors. Modelling of JET Diagnostics Using Bayesian Graphical Models. *Contributions to Plasma Physics*, 51(2-3):152–157, mar 2011.

[20] I Abramovic, A Pavone, D Moseev, N Lopes Cardozo, M Salewski, and HP Laqua. Forward modelling of Collective Thomson Scattering for Wendelstein 7-X plasmas: electrostatic approximation. *submitted to CPC*, 2018.

[21] J van den Berg, I Abramovic, N Lopes Cardozo, and D Moseev. Fast Analysis of Collective Thomson Scattering Spectra on Wendelstein 7-X. *submitted to RSI*, 2018.

[22] V. Erckmann, P. Brand, H. Braune, G. Dammertz, G. Gantenbein, W. Kasparek, H. P. Laqua, H. Maassberg, N. B. Marushchenko, G. Michel, M. Thumm, Y. Turkin, M. Weissgerber, and A. Weller. Electron Cyclotron Heating for W7-X: Physics and Technology. *Fusion Science and Technology*, 52(2):291–312, aug 2007.

[23] V. Erckmann, P. Brand, H. Braune, G. Dammertz, G. Gantenbein, W. Kasparek, H. P. Laqua, G. Michel, M. Thumm, and M. Weissgerber. The 140 GHz, 10 MW, CW ECRH Plant for W7-X: A Training Field for ITER. In *Fusion Energy 2006*, pages IT/2–4Rd, Chengdu, 2007. International Atomic Energy Agency.

[24] Georg Michel, Volker Erckmann, Frank Hollmann, Lothar Jonitz, Walter Kasparek, Heinrich Laqua, Carsten Lechte, Nikolai Marushchenko, Burkhard Plaum, Yuriy Turkin, and Michael Weißgerber. Matching of the ECRH transmission line of W7-X. *Fusion Engineering and Design*, 88(6-8):903–907, oct 2013.

[25] M Stejner, S K Nielsen, S B Korsholm, M Salewski, H Bindslev, V Furtula, F Leipold, F Meo, P K Michelsen, D Moseev, A Bürger, M Kantor, and M de Baar. Collective Thomson scattering

measurements with high frequency resolution at TEXTOR. *Review of Scientific Instruments*, 81(10):10D515, oct 2010.

[26] V Furtula, F Leipold, M Salewski, P K Michelsen, S B Korsholm, F Meo, D Moseev, S K Nielsen, M Stejner, and T Johansen. Performance measurements of the collective Thomson scattering receiver at ASDEX Upgrade. *Journal of Instrumentation*, 7(02):C02039–C02039, feb 2012.

[27] D. Moseev, H. P. Laqua, S. Marsen, T. Stange, H. Braune, V. Erckmann, F. Gellert, and J. W. Oosterbeek. Absolute calibration of sniffer probes on Wendelstein 7-X. *Review of Scientific Instruments*, 87(8):083505, 2016.

[28] H P Laqua, V Erckmann, and M Hirsch. Distribution of the ECRH stray radiation in fusion devices. In *28th EPS Conference on Contr. Fusion and Plasma Phys.*, number June, page P3.099, 2001.

[29] D. Moseev, H.P. Laqua, S. Marsen, N. Marushchenko, T. Stange, H. Braune, F. Gellert, M. Hirsch, U. Hoefel, J. Knauer, J.W. Oosterbeek, Y. Turkin, and The Wendelstein 7-X Team. Inference of the microwave absorption coefficient from stray radiation measurements in Wendelstein 7-X. *Nuclear Fusion*, 57(3):036013, mar 2017.